31st International Conference Nuclear Energy for New Europe
NENE 2022 September 12-15 PORTOROŽ SLOVENIA

Design of an Automated System for Electrolytic Fusion Fuel Implantation in Metallic Filaments

Yannick Verbelen
Interface Analysis Centre, University of Bristol
H.H. Wills Physics Laboratory, Tyndall Ave.
BS8 1TL Bristol, United Kingdom
yannick.verbelen@bristol.ac.uk

Mahmoud Bakr Arby, Tom Wallace-Smith, Thomas B. Scott
Interface Analysis Centre, University of Bristol
H.H. Wills Physics Laboratory, Tyndall Ave.
BS8 1TL Bristol, United Kingdom
mahmoud.bakrarby@bristol.ac.uk, tw17227@bristol.ac.uk, t.b.scott@bristol.ac.uk

ABSTRACT

The probability of nuclear fusion events occurring in inertial electrostatic confined (IEC) fusors is proportional to the fuel density, which requires a tightly controlled partial gas pressure of fuels such as hydrogen isotopes and/or $^{3}\mathrm{He}$. It has been observed experimentally that fusion can also occur as a surface effect if fuel is immobilised in close proximity to the surface of the electrodes, a solid-state approach to increasing fuel density. This raises an engineering challenge to load nuclear fuels into metallic electrode material, in particular metals with a low cross section for neutron capture, such as Zr. Electrolytic implantation of hydrogen isotopes through electrolysis of (heavy) water offers a convenient engineering pathway, however, previous work has shown that it is challenging to achieve consistent, homogeneous, and reproducible results using electrolysis relying on static electrodes. The presented apparatus offers a solution to the implantation problem that is usable with any metallic filament and $^{2}\mathrm{H}$ as fuel by running a wire cathode dynamically through the centre of a cylindrical anode. The system was modelled to enable configurable implantation depth as a function of current and feed rate.

1 INTRODUCTION

A traditional Farnsworth-Hirsch fusor uses electrostatic confinement rather than electromagnetic confinement of plasma, relying on the electric field between electrodes to ionise a gaseous fuel in a vacuum environment [1]. The ionised fuel with positive electric charge is then accelerated towards the negative electrode, in most fusor designs a wire sphere in the centre of the chamber. As ions are accelerated to the centre electrode from opposite sides of the chamber, there is a possibility of collision near the centre. It is possible for ions to undergo nuclear fusion, and for light isotopes such as $^{2}\mathrm{H}$, $^{3}\mathrm{H}$, and $^{3}\mathrm{He}$, an electric field in excess of ca. $25\,\mathrm{kV}$ is already enough to overcome the repelling electric force between identical electrically polarised ions [2]. The plasma density is the most important trade-off in the design, if the objective is to achieve

a neutron or X-ray output as high as possible. Higher plasma density increases the probability of ions colliding and fusing, however, it also decreases the mean free path for accelerating ions. If collisions occur before the energy necessary to fuse is reached, fusion will not occur. This problem can be partially offset by increasing the voltage, which then permits colliding ions to lose some of their energy and still retain sufficient kinetic energy to fuse. In practice, high voltages lead to arcing in the electrically conductive plasma, which makes it difficult to increase the neutron output of designs based on the Farnsworth-Hirsch concept beyond 10^7–10^8 n/s.

A promising solution to this practical engineering limitation is to confine half of the fuel as a solid-state target [3]. This approach is more akin a conventional particle accelerator where protons or electrons are accelerated towards a stationary target such as tungsten to produce X-rays or gamma rays with a desired energy spectrum. Hence, if the potential is doubled to a minimum of ca. $40\,\mathrm{kV}$, fusion can theoretically occur between an accelerated hydrogen or helium ion and a statically confined hydrogen or helium atom [4, 5]. Bowden-Reid et al. estimate that 80% of fusion events could be a result of such lattice confined fuel [5]. Mean free path limitations cause near-instant loss of kinetic energy when charged particles enter solids, which limits fusion with solid-state targets largely to a surface or slightly sub-surface phenomenon. It is therefore desirable to maximise the ratio between fuel atoms and metal atoms on the surface of the electrode. In this work, a computer controlled system is introduced to control the depth of deuterium implantation in metallic filaments such as Zr used in the construction of IEC fusor electrodes for lattice confined fusion (LCF).

2 PREVIOUS WORK

Uniformly implanting hydrogen isotopes into a metallic filament target requires the entire filament as cathode to be equidistant to the anode at any time. This effect is achieved in conventional electrolysis configurations using established parallel plate electrodes. This approach has 2 drawbacks: firstly, it is fundamentally a batch process that is not easily suited to long filament sections without requiring a large volume of electrolyte, which in the case of heavy water is expensive. Secondly, in a parallel plate configuration, only one side of the filament is facing the other electrode, which leads to implantation results with a heterogeneous cross section.

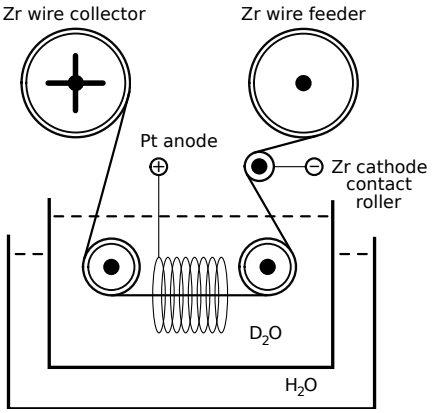

Figure 1: Symbolic layout of a concentric electrolysis prototype for deuterium implantation in wires, proposed in [3], reproduced with permission.

Verbelen et al. (2021) observed this problem using SIMS analysis of implanted samples. In [3], they suggest an alternative approach which can potentially solve these problems, using a cylindrical Pt anode wire and Zr cathode target passing through the centre line of the cylindrical

anode, shown in Fig. 1. Presented here is the first prototype of the novel approach, designed for electrolytic deuterium implantation in metallic filaments through electrolysis of heavy water.

3 PROTOTYPE IMPLEMENTATION

The prototype is constructed as a single assembly consisting of a machined and folded U-shaped frame with inner spacing of 80 mm, manufactured in 6061 aluminium alloy and anodised to improve chemical resistance. Spools and pulleys are mounted on perpendicular shafts, secured with circlips. The prototype is shown in Fig. 2. All shafts are machined in PEEK to ensure proper electrical insulation between filament and metal frame.

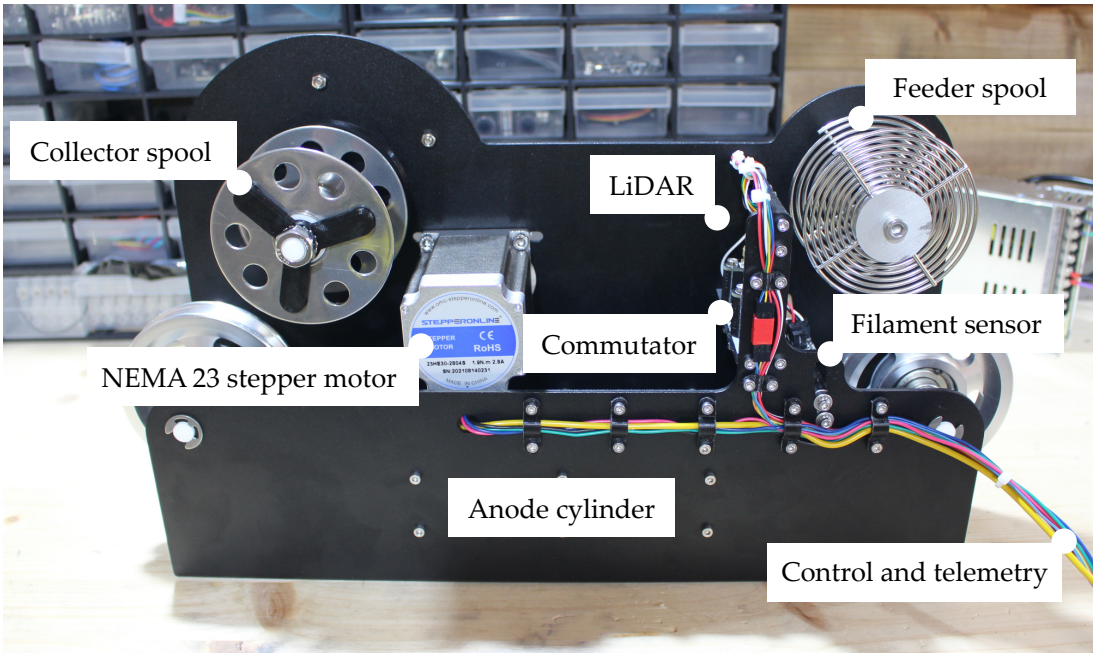

Figure 2: Prototype without heavy water tank, with some of the functional components identified. Dimensions are 450 mm by 95 mm, with a height of 240 mm.

Filament is loaded onto the feeder spool (top right) which is monitored by a LiDAR unit to compensate for variations in spool diameter. The filament is passed over the commutator, a pulley with V-groove mounted on a brass shaft, supported on either side by a 3 mm bearing, and electrically interfaced with a 5 mm thick carbon brush to transfer electrical current to the moving filament. The filament passes through a photo-interrupter as filament sensor, and is looped back through the anode cylinder. The anode cylinder consists of a nickel coated steel mesh with inner diameter of 48 mm and length 150 mm, shown in Fig. 3. The filament is kept centered in the anode cylinder using 2 free-running pulleys of 100 mm diameter on either side of the assembly. The treated filament is finally collected on the collector spool (top left) which is driven by a NEMA 23 stepper motor for accurate control of the feed rate.

4 TELEMETRY AND CONTROL

The organisation of sensors and actuators is shown in Fig. 4. The system is based around an RP2040 microcontroller programmed in C++ through the Arduino software development framework. The sensor inputs, shown to the left, are used to regulate current and filament feed rate. The control interface consists of tactile buttons that enable the user to set a desired

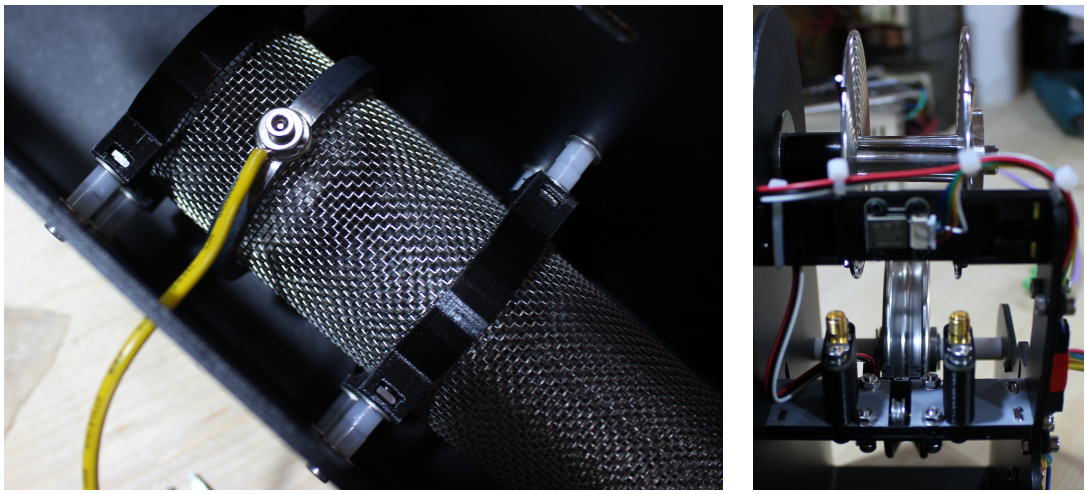

Figure 3: Left: close-up of the wire mesh cathode cylinder, supported by ABS brackets providing electrical isolation. The cathode wire is connected with a machined conductive collet. Right: commutator assembly with V-pulley visible at the bottom and SMA electrode terminals with integrated carbon brushes. ToF400F LiDAR targeting feeder spool on the top horizontal beam.

implantation depth. Feedback is provided to the user with an integrated LCD display on the control interface.

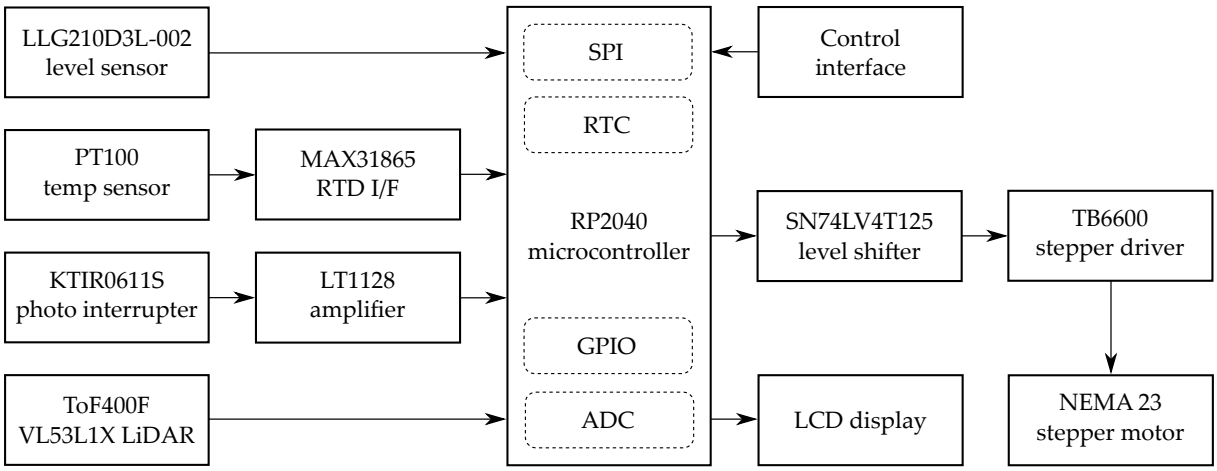

Figure 4: Block diagram of the electronic control unit, featuring telemetry and user interface.

4.1 Electrolyte monitoring

In a glass tank with low thermal conductivity, the temperature of the electrolyte increases over time, particularly at higher current densities. When operating in constant voltage mode (CV), a negative feedback effect exists because residual oxygen gas bubbles cause a negative void coefficient, i.e. they displace electrolyte which increases electrolyte impedance, which in turn decreases the current and power dissipation. Running in CV mode is disadvantageous from a control perspective however, because keeping the voltage constant leaves the current variable. Consequentially, the current density is variable, which complicates calculation of effective hydrogen implantation depth, and requires dynamic adjustments of wire speed. Constant current

(CC) mode is therefore the preferred operation mode, because current density is constant and wire speed can also be kept constant. Unfortunately, in CC mode, the void coefficient is positive: as oxygen bubbles form and displace electrolyte, current is forced through the remaining electrolyte which increases in temperature. As impedance increases with temperature above freezing point [6], a higher power will be forced through the electrolyser in CC mode, which causes the electrolyte to heat up further until boiling [3]. At this point, steam bubbles cause further displacement of liquid electrolyte and the reactivity coefficient becomes strongly positive, quickly boiling off the remaining electrolyte if no action is taken. The presented system counteracts the thermal runaway in CC mode by monitoring electrolyte level and temperature separately.

4.1.1 Thermal monitoring

A PT100 platinum RTD is used as temperature sensor, according to IEC751, with specification $\alpha = 3.85\,\mathrm{m\Omega/\Omega/^\circ C}$. The body of the sensor is in direct contact with the KOH electrolyte, and manufactured from 316L stainless steel. The operating temperature of the PT100 sensor is in the range of $-200\,^\circ\mathrm{C}$ – $650\,^\circ\mathrm{C}$, which is more than sufficient for the application since the electrolyser is designed to operate between room temperature ($20\,^\circ\mathrm{C}$) and the boiling point of $0.1\,\mathrm{M}$ KOH in water at $79\,^\circ\mathrm{C}$. The analog to digital interface of the PT100 sensor is implemented with a Maxim Integrated dedicated RTD-to-digital front-end [7]. This device is interfaced over a serial bus (SPI) with $3.3\,\mathrm{V}$ signaling levels, and is specifically designed for use with PT100 and PT1000 RTDs in industrial applications. With a 15-bit ADC its theoretical nominal temperature resolution is $0.031\,25\,^\circ\mathrm{C}$, but the actual accuracy over its operating conditions is $\pm 0.5\,^\circ\mathrm{C}$ which is sufficient for this application.

4.2 Filament monitoring

The position of the filament and feed rate are critical parameters and must be recorded with the highest achievable accuracy. Uniformity of deuterium implantation relies on mechanical constraints, i.e. the filament running through the exact centre line of the mesh electrode cylinder. If deviations occur, for example because of insufficient tension on the filament, the current density on the filament surface will become heterogeneous. In a worst-case scenario, large deviations may result in electrical contact between filament and electrode cylinder, causing short-circuit.

4.2.1 Feed rate compensation

The drive mechanism rotates the collector spool at a constant angular velocity. As filament accumulates on the collector spool, the effective diameter of the spool that filament is spun onto slowly increases because fresh filament is spun over previously collected filament. It is inevitable that the effective feed rate of the filament speeds up as more filament is collected on the spool, which induces an error gradually decreasing implantation depth. The effect is more profound for long sections requiring larger spool diameters: an empty collection spool has a diameter of $28\,\mathrm{mm}$, which at an angular velocity of 1 RPM corresponds to a feed rate of $1.3\,\mathrm{mm\,s^{-1}}$. At maximum capacity however, the collection spool has a diameter of $80\,\mathrm{mm}$ which at the same angular velocity results in a filament feed rate of $4.2\,\mathrm{mm\,s^{-1}}$. It will be clear that an actual feed rate variation of a factor 3 is not acceptable, and must be compensated for.

The implemented solution uses a time-of-flight sensor of type TOF400F, which features a solid-state VL53L1X LiDAR from ST Microelectronics that can be configured for a maximum

range between $90\,\mathrm{cm}$ [8] up to $4\,\mathrm{m}$ [9]. It uses a $940\,\mathrm{nm}$ (infrared) laser with optical filters, and has a field of view of $27°$. The absolute error on measurements under ambient light conditions is $\pm 25\,\mathrm{mm}$, and measurements are fed into an array used to compute a moving average to obtain more accurate distance measurements. A software library provided by ST Microelectronics was used to read out the SPAD sensor array and process the measurements. The measured spool diameter is then used to correct the filament feed rate. The compensation equation is

$$\phi_1 = \frac{L_F}{L_C} \frac{D_0}{D_0 - 2(\beta_0 - \beta_1)} \phi_0 \tag{1}$$

where ϕ_0 is initial angular feed rate and ϕ_1 is angular feed rate at time t_1, L_F and L_C are the widths of the feeder and collector spools respectively, β_0 is the initial distance measured by the LiDAR and β_1 is the distance measured at time t_1, and D_0 is the initial diameter of the feed spool.

4.2.2 Filament positioning and tensioning

The filament must remain under adequate tension at all times, not only to ensure alignment with electrode center line, but also to prevent it from slipping off the pulleys, and to establish a proper electrical contact between filament and electrical drive pulley. The position of the filament is measured by a photo-interrupter of type KTIR0611S manufactured by Kingbright, which consists of an infrared emitter and phototransistor positioned face to face, with the filament passing between them. If the filament is correctly tensioned and positioned, it absorbs a constant fraction of the emitted infrared light, and the photo-current is constant. In case it runs off the pulleys, snaps, or is incorrectly tensioned, changes in current can be observed on the phototransistor side which triggers and alarm. The photo-interrupter module was assembled by CNC-Planet, UK.

4.3 Drive mechanism

The drive mechanism consists of a shaft with collector spool driven by a 100-tooth GT2 drive pulley, linked with a $6\,\mathrm{mm}$ GT2 synchronous belt to a stepper motor with 20-tooth GT2 drive pulley. The stepper motor is a NEMA 23 motor with maximum torque of $1.9\,\mathrm{N\,m}$ at a winding current of $2.8\,\mathrm{A}$. The implemented model is 23HE30-2804S manufactured by Stepper-Online. In an effort to minimise design complexity, there is no idler pulley on the belt, instead longitudinal slots are provisioned in the mounting panel so allow belt tensioning during assembly. The stepper driver is a TB6600 general purpose CNC stepper motor controller supplied by CNC-Planet, UK. It supports microstepping at a resolution of 6400 steps per revolution (microstepping mode 32), which corresponds to an actual resolution of 32,000 steps per revolution due to the 1:5 GT2 belt reduction. At the maximum collector spool diameter of $80\,\mathrm{mm}$, this yields an effective filament position resolution of $7.6\,\mu\mathrm{m}$ per step.

5 IMPLANTATION DEPTH

The depth of implantation is proportional to the number of deuterium ions implanted into the filament surface. It is proportional to the current, an inversely proportional to the feed rate V_f, i.e. the speed with which the filament is passing through the electrolysis section. The implantation rate σ_I can be expressed as

$$\sigma_I = \frac{I \eta_I \eta_E}{L \pi d e N_A} \tag{2}$$

where I is the electric current, η_I and η_E the efficiencies of implantation and electrolysis respectively (η_E is approx 40–70% for alkaline water baths) [10], L is the length of the section, d diameter of the filament, e the elementary charge ($e = 1.602 \times 10^{-19}\,\mathrm{C}$) [11], and N_A Avogadro's constant ($N_A = 6.022 \times 10^{23}\,\mathrm{mol}^{-1}$) [12]. The unit of σ_I is mol/s/mm^2.

For a given feed rate V_f, the time t to traverse the electrolysis section is

$$t = \frac{L}{V_f} \tag{3}$$

Which, substituted in the equation for σ_I, gives a value for implantation depth Θ_I in mol per mm^2:

$$\Theta_I = \frac{I\eta_I\eta_E}{V_f \pi d e N_A} \tag{4}$$

Note that the length of the electrolysis section is no longer present as a parameter in this equation because the current I is assumed to be distributed uniformly over the entire section. The concentration of deuterium ions in the filament leaving the electrolysis section is only function of the current and the feed rate.

6 CONCLUSIONS AND FUTURE WORK

This work presents the construction and telemetrisation of an integrated prototype specifically designed to facilitate controlled implantation of deuterium ions into metallic filaments through electrolysis of heavy water. The prototype, designed to be partially submerged in a tank of heavy water, is optimised to pass a filament used as electrical cathode through a cylindrical anode to achieve uniform implantation on the entire filament surface. A user interface allows implementation depth to be configured dynamically. The software running the control system uses telemetry inputs to compute the matching filament feed rate and drive a stepper motor to achieve the configured implantation depth. Models for feed rate calculations are presented in this work, and have been implemented in software to automate the implantation process.

The prototype was found to behave as expected during 'dry' test runs to validate mechanical integrity of the assembly and verify actual filament feed rates set in software. The authors aim to proceed with deuterium implantation experiments in zirconium wire as soon as sufficient quantities of heavy water can be acquired. Further SIMS analysis on the produced samples will then reveal whether the presented prototype implementation satisfies its design requirements.

ACKNOWLEDGMENTS

The authors extend their gratitude to Miss Sofia Leadbetter of the National Nuclear User Facility for Hot Robotics (NNUF-HR)[1], for logistic support provided to the project. The authors also thank the PCBWAY team[2] for their excellence in machining the most complex mechanical parts critical to the success of the assembly, and for providing the circuit boards to support the control electronics.

[1] https://www.nnuf.ac.uk

[2] https://www.pcbway.com

REFERENCES

[1] Robert L Hirsch. Inertial-electrostatic confinement of ionized fusion gases. *Journal of applied physics*, 38(11):4522–4534, 1967.

[2] George H Miley and S Krupakar Murali. Inertial electrostatic confinement (IEC) fusion. *Fundamentals and Applications*, 2014.

[3] Yannick Verbelen, Tom Wallace-Smith, Kasia Clarke, Yoshiyuki Takahashi, and Tom B. Scott. Power supply design for electrolytic deuterium implantation in zirconium. In *2021 International Conference on Electrical, Computer, Communications and Mechatronics Engineering (ICECCME)*, pages 1–6, 2021.

[4] Bruce M. Steinetz, Theresa L. Benyo, Arnon Chait, Robert C. Hendricks, Lawrence P. Forsley, Bayarbadrakh Baramsai, Philip B. Ugorowski, Michael D. Becks, Vladimir Pines, Marianna Pines, Richard E. Martin, Nicholas Penney, Gustave C. Fralick, and Carl E. Sandifer. Novel nuclear reactions observed in bremsstrahlung-irradiated deuterated metals. *Phys. Rev. C*, 101:044610, Apr 2020.

[5] Richard Bowden-Reid, Joe Khachan, Jan-Philipp Wulfkühler, and Martin Tajmar. Evidence for surface fusion in inertial electrostatic confinement devices. *Physics of Plasmas*, 25(11):112702, 2018.

[6] Kai An, Pallab Barai, Kandler Smith, and Partha Mukherjee. Probing the thermal implications in mechanical degradation of lithium-ion battery electrodes. *Journal of the Electrochemical Society*, 161:A1058–A1070, 04 2014.

[7] Anjali Rai and Deepak Yadav. Evaluating wiring configurations for RTD sensor in temperature measurement. *I-Manager's Journal on Electronics Engineering*, 10(1):1, 2019.

[8] Stefan M Rizanov and Peter I Yakimov. Cattle disease detecting IoT thermographic system. In *2021 XXX International Scientific Conference Electronics (ET)*, pages 1–6. IEEE, 2021.

[9] Ander Galisteo, Qing Wang, Aniruddha Deshpande, Marco Zuniga, and Domenico Giustiniano. Follow that light: Leveraging leds for relative two-dimensional localization. In *Proceedings of the 13th International Conference on emerging Networking EXperiments and Technologies*, pages 187–198, 2017.

[10] MD Rashid, Mohammed K Al Mesfer, Hamid Naseem, and Mohd Danish. Hydrogen production by water electrolysis: a review of alkaline water electrolysis, pem water electrolysis and high temperature water electrolysis. *International Journal of Engineering and Advanced Technology*, 2015.

[11] Beat Jeckelmann and François Piquemal. The elementary charge for the definition and realization of the ampere. *Annalen der Physik*, 531(5):1800389, 2019.

[12] RO Davies. Avogadro's number and Avogadro's constant. *Physics Education*, 8(4):275, 1973.